Chiral metamirrors for broadband spin-selective absorption

Liqiao Jing, Zuojia Wang, Yihao Yang, Bin Zheng, Yongmin Liu, and Hongsheng Chen

Citation: Appl. Phys. Lett. **110**, 231103 (2017); doi: 10.1063/1.4985132
View online: http://dx.doi.org/10.1063/1.4985132
View Table of Contents: http://aip.scitation.org/toc/apl/110/23
Published by the American Institute of Physics

Chiral metamirrors for broadband spin-selective absorption

Liqiao Jing,[1,2,a)] Zuojia Wang,[1,2,3,a),b)] Yihao Yang,[1,2] Bin Zheng,[1,2] Yongmin Liu,[4] and Hongsheng Chen[1,2,b)]

[1]*State Key Laboratory of Modern Optical Instrumentations, Zhejiang University, Hangzhou 310027, China*
[2]*The Electromagnetics Academy at Zhejiang University, Zhejiang University, Hangzhou 310027, China*
[3]*School of Information Science and Engineering, Shandong University, Jinan 250100, China*
[4]*Department of Mechanical and Industrial Engineering, Department of Electrical and Computer Engineering, Northeastern University, Boston, Massachusetts 02115, USA*

(Received 28 March 2017; accepted 25 May 2017; published online 7 June 2017)

Chiral metamirrors are recently proposed metadevices that have the ability of selective reflection for the designated circularly polarized waves. However, previous chiral metamirrors only work in a narrow band, which would limit their potential applications in engineering. Here, we propose an approach towards broadband spin-selective absorption. By combining the chiral resonant modes of two asymmetric split-ring resonators, we design and construct a chiral metamirror that absorbs only the left-handed circularly waves over a broad frequency range. The measured results show a bandwidth of 5.1%, almost 96% larger than that of the narrowband metamirror. Furthermore, the proposed chiral metamirror exhibits prominent performance at oblique incidence, even when high-order diffraction appears. The total thickness of the metamirror is only one-ninth of the wavelength, highly suitable for on-chip integration. Our findings may provide an efficient approach to boost the working bandwidth of the chiral metamirror and could advance its applications in optical instruments. *Published by AIP Publishing.* [http://dx.doi.org/10.1063/1.4985132]

Chirality refers to the geometry of an object lacking any mirror symmetry plane and it widely exists in nature, ranging from molecules, to proteins, and to crystals.[1] This feature contributes to various chiroptical phenomena such as optical activity and circular dichroism, which are of great importance in the structural characterization and spectroscopy of chemical and biomolecular substances. Over the past few years, chiral metamaterials have attracted tremendous attention due to their strong chiroptical effects with magnitudes much larger than that in natural materials.[2] By properly designing the arrangement of plasmonic inclusions, researchers have realized a number of intriguing optical phenomena including chirality-induced negative refraction,[3–7] giant optical activity,[8–11] broadband circular polarizers,[12,13] extrinsic chirality,[14] transmission spin-selective absorbers,[15] and asymmetric transmission.[16–18] Moreover, superchiral electromagnetic fields in chiral plasmonic structures are expected to efficiently enhance the light-mater interaction and thereafter provide an avenue towards high-sensitive chiroptical detection for chiral molecules.[19–21] As two-dimensional counterparts of metamaterials, metasurfaces recently provide a distinct way to manipulate the flow of circularly polarized light.[22] In metasurfaces, the optical responses are controlled by spatially modulating the phase responses of metamolecules. Metasurface-based optical devices such as vortex plates,[23] wave plates,[24] and focusing lenses[25,26] have been realized for both linearly and circularly polarized light. Metasurfaces can effectively tailor the polarization,[27–29] persevere the handedness in reflection,[30] control the ray trajectory of circularly polarized light,[31–33] and manipulate the electron-induced emission.[34] Besides, metasurfaces have also been employed to control near-field waves, such as directional coupling of surface plasmon polaritons.[35,36] These demonstrated metasurfaces so far modulate the amplitude and/or phase for both left-handed circularly polarized (LCP) and right-handed circularly polarized (RCP) light with equal efficiency.

Recently, chiral metamirrors have been proposed to manipulate the extinction of circularly polarized light in reflection.[37,38] When unpolarized light impinges onto such metamirrors, photons with different spin states will undergo different extinction and thereafter the metamirrors could reflect only one kind of circularly polarized light, resulting in an almost perfect extinction ratio. The general method to achieve this chiroptical response has been investigated by symmetry considerations,[37] and experimental verification has also been implemented in both microwave and near-infrared regimes.[38,39] The near-perfect extinction in chiral metamirrors provides us an efficient way to design ultracompact circularly polarized light detectors, while the property of preservation in handedness may find fascinating applications in chiral cavities or spin lasers. However, current chiral metamirrors are mainly based on resonant plasmonic structures and only show a narrowband chiroptical response. Therefore, how to design chiral metamirrors with improved performance in bandwidth is a crucial and urgent issue to be solved.

In this letter, we experimentally demonstrate a chiral metamirror with broadband performance, which enables spin-selective absorption of circularly polarized waves. According to the general design methodology,[37] we design an asymmetric split-ring resonator (ASRR) to break both the n-fold ($n > 2$) rotational and mirror symmetries. Two ASRRs with different geometric parameters are integrated into a

[a)]L. Jing and Z. Wang contributed equally to this work.
[b)]Authors to whom correspondence should be addressed: z.wang@sdu.edu.cn and hansomchen@zju.edu.cn

single unit cell to achieve broadband chiral responses. When the resonant frequencies are close enough, the resonant modes of the adjacent ASRRs could couple together and thereby result in a broadband spectrum of spin-selective absorption. Simulation results show a maximum absorption of 95.2% and a full width at half maximum (FWHM) of 5.7% (0.56 GHz) for the absorption of left-handed circularly polarized (LCP) waves, while the absorption of the other spin state is kept smaller than 19.5%. The experimental verification is implemented at microwave frequencies and the measured results match well with the simulation ones. The angular sensitivity has also been investigated and the chiral metamirror maintains very good performance as the incident angle increases. The thickness of the proposed chiral metamirror is only one-tenth wavelength, and hence, it is highly desirable for on-chip integration. Such metamirrors could promise a variety of applications, such as polarimetric imaging and polarization-sensitive detection of electromagnetic waves.

The schematic of the chiral metamirror is illustrated in Fig. 1. Conventional metallic mirrors reverse the handedness of circularly polarized waves upon reflection, because the boundary condition requires the in-plane electric fields to change a phase of π and the wave vector flips the direction. This feature increases the complexity of optical instruments or systems for circularly polarized waves, and hence, many researchers have tried to design mirrors without this drawback. For instance, one can obtain anisotropic handedness-preserving mirrors by combining the metallic "electric mirrors" with the metamaterial-based "magnetic mirrors."[40] The functionality of the chiral metamirrors, in contrast, is to preserve the handedness of a designated circularly polarized wave upon reflection while totally absorb the other spin state. Such spin-selective metamirrors can be considered as an integration of a reflective polarizer and a filter. Here, we assume that the right-handed circularly polarized (RCP) waves are largely reflected and label them as "R-type" metamirrors. The key for the realization of such metamirrors is a chiral subwavelength structure which should simultaneously break the n-fold ($n > 2$) rotational and mirror symmetries.[37] According to this principle, we adopt ASRRs as the resonant elements, as shown in Fig. 1(b). Each ASRR is composed of a G-shape structure and a C-shape one. The dimensions of the two ASRRs are $s = 1$ mm, $l_1 = 4$ mm, $l_2 = 4.3$ mm, $g_1 = g_2 = 1$ mm, $g_3 = 1.5$ mm, $R_1 = 2.3$ mm, $R_2 = 2.2$ mm, and

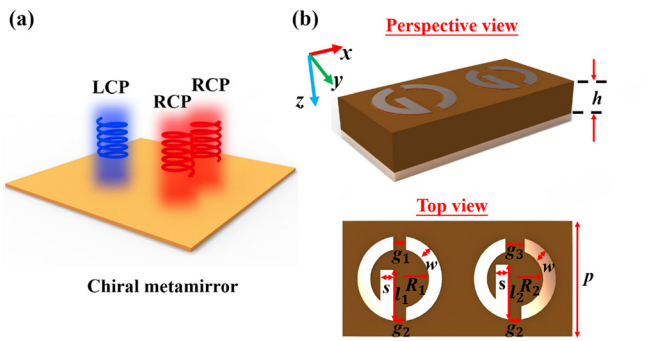

FIG. 1. (a) The schematic of the chiral metamirror. R-type metamirror reflects RCP waves with preserved handedness, while absorbs the other spin state. (b) A unit cell of the ASRR chiral metamirror.

$w = 1$ mm. The periodicities of the unit cell are $p_x = 18$ mm and $p_y = 9$ mm in the x and y directions, respectively. FR4 is selected as the dielectric spacer with the relative permittivity of 4.2 and the loss tangent of 0.025, and its thickness is optimized to 3.1 mm. A homogeneous metallic layer is placed at the bottom to realize zero transmission. The metal here is copper with conductivity $\sigma = 5.8 \times 10^7$ S/m and thickness of 0.105 mm. Hence, the total thickness is 3.31 mm, which is only about one-ninth of the wavelength at 10 GHz.

We have performed full-wave numerical simulations (CST Microwave Studio) to validate the functionality of the chiral metamirror. First, narrowband metamirrors are investigated to find appropriate geometries of the meta-atoms. Figure 2(a) shows the absorption spectra of the two individual ASRR metamirrors (ASRR1 and ASRR2). One can see that the FWHMs of the ASRR1 and ASRR2 are 2.6% (0.25 GHz) and 3.2% (0.32 GHz) with the resonant peaks at 9.45 GHz and 9.99 GHz, respectively. However, the bandwidths of both structures are narrow. Consequently, combining individual chiral structures together is expected to expand the bandwidth performance. The solid line indicates that the FWHM of the double-ASRR metamirror is about 5.7% (0.56 GHz) for the absorption of LCP waves, with the maximum absorption reaching 95.2%. Meanwhile, the absorption of RCP waves is dramatically suppressed and always kept smaller than 20% over a broad frequency range. The bandwidth of the double-ASRR metamirror is almost 119% and 78% broader than those of the ASRR1 and ASRR2 metamirrors, respectively. From the reflection spectra shown in Fig. 2(b), we see that under RCP incidence, the magnitude ratio of the reflected RCP (r_{RR}) to the reflected LCP waves (r_{LR}) is high over a broadband region. Therefore, not only can the proposed metamirror selectively reflect LCP waves with high efficiency but also the handedness can be well preserved.

We have investigated the dependence of absorption spectra on the geometric parameters of the meta-atoms, in order to see how the change in the distance between two

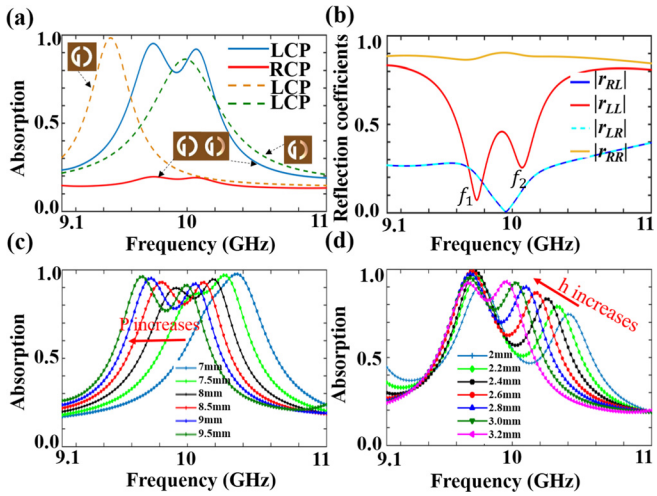

FIG. 2. Simulation results of the chiral metamirrors. The absorption spectra of the ASRR1 (orange dashed line), the ASRR2 (green dashed line), and the double-ASRR metamirrors. (b) Reflection spectra of the double-ASRR metamirror. Dependence of the absorption spectra on the period P (c) and dielectric spacer h.

resonators affects the near-field coupling and the spectral response. The dependence of the chiral performance on the period p_y is plotted in Fig. 2(c). As the period p_y increases from 7 mm to 9.5 mm, the absorption band is gradually broadened and undergoes certain redshifts. For even larger periods, two resonant frequencies couple weaker and the average absorption decays in the band. In all cases, the period in the x direction is kept to two times of that in the y direction ($p_x = 2p_y$). Besides, we have also investigated the influence of the thickness of the dielectric spacer on the chiroptical responses. As shown in Fig. 2(d), the second resonant peak redshifts significantly when the thickness is increased from 2 mm to 3.2 mm. However, the first absorption peak is not largely affected by varying the thickness of the dielectric spacer.

To further understand the origin of the resonances, the surface current distributions at the resonant frequencies are plotted in Fig. 3. Due to the asymmetric feature of the ASRR structure, LCP and RCP waves induce distinct surface current distributions on the two arms. It is clearly observed that LCP illuminations can induce stronger surface currents on the metallic surface and result in the strong spin-selective absorption. More interestingly, at the first resonant frequency of 9.74 GHz, the surface currents on the two arms oscillate in the opposite directions and the resonance behaves like a combination of strong magnetic and weak electric dipoles. At the second resonant frequency of 10.04 GHz, the surface currents oscillate in the same direction and they work like the combination of weak magnetic and strong electric dipoles. The breaking of mirror symmetry influences the dipole interactions and the overall electromagnetic responses behave like Fano resonances.

To experimentally realize the chiral metamirror, we perform a series of experiments in the microwave region. Based on the available printed circuit board (PCB) technology, the chiral metamirror has been fabricated with the same parameters taken in the above simulations. The experimental setup includes an Agilent Vector Network Analyzer and two broadband microwave antennas. Microwave absorbing foams are placed around the sample to reduce the scattering from the edges of the measurement platform. The metamirror consisting of 16×32 unit cells are designed and its overall area is $288 \times 288\,\text{mm}^2$ as shown in Fig. 4(a). The signals from these antennas are linearly polarized, so the linear reflection coefficients r_{xx}, r_{xy}, r_{yx}, and r_{yy} are measured, in which the first subscript indicates the polarization of the

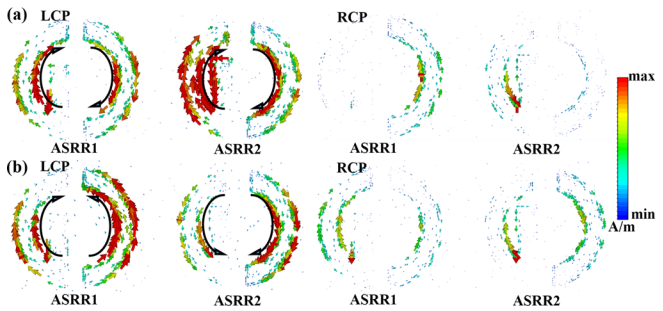

FIG. 3. Surface current distributions on the metallic ASRRs at the resonance frequencies of (a) 9.74 GHz and (b) 10.04 GHz, respectively.

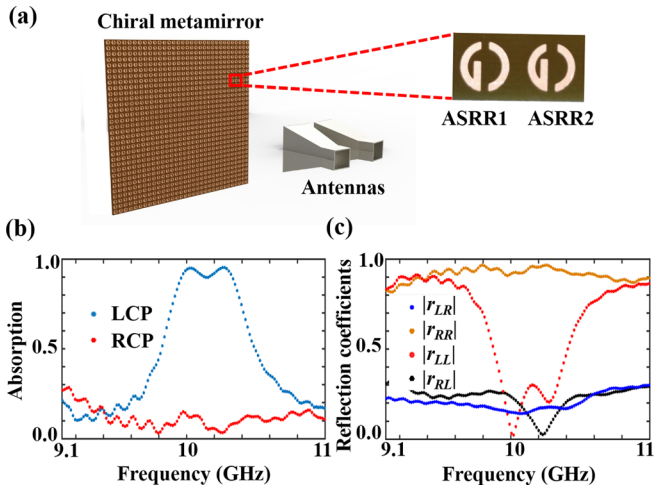

FIG. 4. (a) Schematic of the experimental setup with linear antennas and photographs of the fabricated sample. The circular dichroism metamirror contains 16×32 unit cells and its overall area is $288 \times 288\,\text{mm}^2$. The zoom-in picture is the photograph of a unit cell. (b) Measured absorption spectra and (c) reflection coefficients of the chiral metamirror at normal incidence.

reflected field (x-polarization or y-polarization) and the second subscript corresponds to the polarization of the incident field. Therefore, the reflection matrix for circularly polarized waves can be obtained from the linear reflection coefficients using the following equation:

$$\begin{pmatrix} r_{++} & r_{+-} \\ r_{-+} & r_{--} \end{pmatrix} = \frac{1}{2} \times \begin{pmatrix} (r_{xx}+r_{yy})+i(r_{xy}-r_{yx}) & (r_{xx}-r_{yy})-i(r_{xy}+r_{yx}) \\ (r_{xx}-r_{yy})+i(r_{xy}+r_{yx}) & (r_{xx}+r_{yy})-i(r_{xy}-r_{yx}) \end{pmatrix}.$$

Here, "+" and "−" are defined as the clockwise and counterclockwise circularly polarized waves when viewed along the $+z$ direction, respectively. It is worth noting that each reflection coefficient has different physical meanings compared with transmission cases, because the wave vectors are in opposite directions for transmitted and reflected waves. Here, the incident waves are assumed to propagate along the $+z$ direction. Consequently, the reflection coefficients are defined as $r_{LR} = r_{++}$, $r_{RR} = r_{-+}$, $r_{LL} = r_{+-}$, and $r_{RL} = r_{--}$.[37]

Figure 4(b) shows the measured absorption spectra at microwave frequencies between 9.1 GHz and 11 GHz. As expected, a broadband spin-selective absorption appears. One can see that the FWHM of the chiral metamirror is about 5.1% (0.52 GHz), ranging from 9.89 GHz to 10.41 GHz for LCP waves. It is 96% larger than that of the ASRR1 metamirror. The maximum absorption for LCP waves reaches 95.3%, while almost all the RCP waves are reflected without handedness reversal. By comparing the simulated and experimental results, we can observe that the absorption spectrum for LCP waves undergoes a blue shift. There are two reasons for this phenomenon. One is that PCB fabrication precision is not perfect. The other is the inaccuracy of either the permittivity or the loss tangent of the substrate dielectric. However, the experimentally measured results match well with simulation results. Figure 4(c) plots the amplitude of four reflection coefficients, providing the complete information about how energy is distributed

when the chiral metamirror selectively absorbs one spin state of waves. At 10.02 GHz and 10.26 GHz, the chiral metamirror has two absorption resonances for LCP waves (r_{LL}), while the handedness-preserving reflectivity for RCP waves (r_{RR}) remains high. The black and blue dotted lines indicate that part of the energy is still converted into the cross polarization due to the anisotropy of the structure.

Angular sensitivity is another important property in applications and therefore we next focus on the performance of the designed chiral metamirrors at oblique incidence. To better clarify the angular-dependent performance, we investigate two different cases in which the wave vectors are confined in the *yz*-plane and *xz*-plane, respectively. In the former case, the simulated absorption spectra are plotted in Fig. 5(a). Here, the blue and green curves represent the absorption spectra for LCP waves, while the red and black curves correspond to the RCP counterparts. As the angle of incidence (θ) increases from 30° to 45°, the first chiral absorption peak slightly drops and redshifts, whereas the second peak behaves in the opposite way. This feature results in a broader bandwidth yet a reduction of the average absorption around the resonant frequencies. On the contrary, the absorption performance for RCP waves does not show significant degradation with the maximum absorption still kept smaller than 30%. The measured results are shown in Fig. 5(b), which are highly consistent with the simulated ones. The measured absorption spectra, as mentioned above, also undergo a slight blueshift due to the inaccuracy from either the substrate or the sample fabrication. Although the absorption contrast between LCP and RCP waves still remains high, the ratio between r_{RR} and r_{LR} largely decreases. It means that, as the angle of incidence

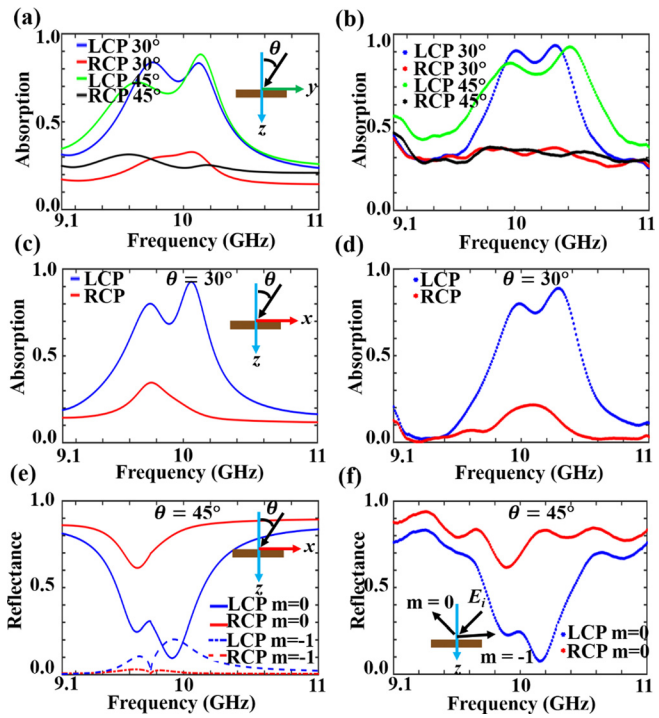

FIG. 5. Optical responses of the chiral metamirror at oblique incidence. (a) Simulated and (b) measured absorption spectra of the chiral metamirror with the wave vectors confined in the *yz*-plane. (c)–(f) The simulated and measured reflection coefficient spectra with the wave vectors confined in the *xz*-plane. (c) and (d) The case of $\theta = 30°$ and (e) and (f) correspond to the case of $\theta = 45°$.

increases, the ability of the chiral metamirror in handedness preservation declines. This is caused by the change in the phase difference between the two spin states, which in turn influences the constructive and instructive interferences of waves. Therefore, more energy is converted to the cross-polarized state.

The other case at oblique incidence is that the wave vectors are confined in the *xz*-plane. For this case, high-order diffraction needs careful consideration because the periodicity of the unit cell in the *x* direction is no longer deep subwavelength. In our case, the periodicity p_y is much smaller than half of the wavelength yet p_x is larger than that. As a result, high-order diffraction can only occur when the incoming waves propagate in the *xz*-plane with a large angle of incidence. In particular, no high-order diffraction exists in the case of $\theta = 30°$, while the first-order diffraction ($m = 1$ or $m = -1$, and $n = 0$) happens in the case of $\theta = 45°$. Figure 5(c) shows the absorption spectra of the chiral metamirror at 30° incidence. Both the simulated and the measured results present good performance on spin-selective absorption and they are highly consistent with each other.

Next, we discuss the case of $\theta = 45°$, in which high-order diffraction needs to be considered. Interestingly, the performance of broadband spin-selective absorption is well preserved for the zero-order diffraction (the normal reflected wave). To better illustrate the influence of the high-order diffraction, we further calculate the reflectance spectra of each diffracted beam, as shown in Fig. 5(e). Blue solid and dashed curves represent the zero- and first-order reflectance for RCP incident waves, respectively. Red solid and dashed curves correspond to the LCP counterparts. Here, the reflectance is calculated by $1 - |r_{LR}|^2 - |r_{RR}|^2$ and $1 - |r_{RL}|^2 - |r_{LL}|^2$ for RCP and LCP waves, respectively. It is worth noting that, for RCP incidence, the reflected power of the first-order diffraction is much lower than the zero-order one. Meanwhile, for LCP incidence, both zero- and first-order diffracted waves are largely suppressed due to the high-efficient absorption. This indicates that the high-order diffraction has almost no influence on the chiroptical performance of the metamirror and it can efficiently absorb LCP waves yet reflect RCP waves without handedness reversal. Due to the weak effect of the high-order diffraction, we only measured the reflectance spectra of the zero-order diffracted wave as a comparison [Fig. 5(f)]. The inset figure depicts the diffraction problem of the concerned case. The zero- and first-order diffracted waves are located on opposite sides of the optical axis. The measured spectra agree very well with the simulated ones.

In summary, we have demonstrated a broadband chiral metamirror both theoretically and experimentally. ASRRs are used as the meta-atoms to break the *n*-fold ($n > 2$) rotational and mirror symmetries. By combining the chiral resonances of two ASRRs together, we achieve the broadband performance of spin-selective absorption. Furthermore, the ratio between co- and cross-polarization energy in reflection is kept at a high level. Hence, the chiral metamirror can work as a broadband polarizer or filter that reflects only one kind of circularly polarized wave without handedness reversal. Experimental results show an FWHM of 0.52 GHz for LCP absorption in the microwave region. In addition, the

double-ASRR metamirror exhibits excellent performance at oblique incidence, even when high-order diffraction appears. The chiral metamirror has a thickness of only one-ninth of the wavelength, and hence, it is highly suitable for on-chip integration. Due to the scaling properties of Maxwell's equations, the proposed strategy can be easily extended to other frequencies. Our findings may provide a methodology for a variety of applications, including polarimetric imaging, molecular spectroscopy, and polarization-sensitive detection of electromagnetic waves.

This work was sponsored by the National Natural Science Foundation of China under Grant Nos. 61625502, 61574127, and 61601408, the ZJNSF under Grant No. LY17F010008, the Postdoctoral Science Foundation of China under Grant No. 2015M581930, the Top-Notch Young Talents Program of China, the Fundamental Research Funds for the Central Universities under Grant No. 2017XZZX008-06, and the Innovation Joint Research Center for Cyber-Physical-Society System. Y.L. acknowledges the partial financial support from the Office of Naval Research under grant number N00014-16-1-2049, and Samsung Global Research Outreach (GRO) Program.

[1]L. D. Barron, *Molecular Light Scattering and Optical Activity* (Cambridge University Press, 2004).
[2]Z. Wang, F. Cheng, T. Winsor, and Y. Liu, Nanotechnology **27**(41), 412001 (2016).
[3]S. Tretyakov, I. Nefedov, A. Sihvola, S. Maslovski, and C. Simovski, J. Electromagnetic Waves Appl. **17**(5), 695–706 (2003).
[4]J. B. Pendry, Science **306**(5700), 1353–1355 (2004).
[5]C. Monzon and D. W. Forester, Phys. Rev. Lett. **95**(12), 123904–124300 (2005).
[6]E. Plum, J. Zhou, J. Dong, V. A. Fedotov, T. Koschny, C. M. Soukoulis, and N. I. Zheludev, Phys. Rev. B: Condens. Matter Mater. Phys. **79**(3), 035407 (2009).
[7]S. Zhang, Y. S. Park, J. Li, X. Lu, W. Zhang, and X. Zhang, Phys. Rev. Lett. **102**(2), 023901 (2009).
[8]A. V. Rogacheva, V. A. Fedotov, A. S. Schwanecke, and N. I. Zheludev, Phys. Rev. Lett. **97**(17), 177401–177404 (2006).
[9]M. Kuwata-Gonokami, N. Saito, Y. Ino, M. Kauranen, K. Jefimovs, T. Vallius, J. Turunen, and Y. Svirko, Phys. Rev. Lett. **95**(22), 227401 (2005).
[10]M. Ren, E. Plum, J. Xu, and N. I. Zheludev, Nat. Commun. **3**(3), 833 (2012).
[11]Y. Cui, L. Kang, S. Lan, S. Rodrigues, and W. Cai, Nano Lett. **14**(2), 1021–1025 (2014).
[12]J. K. Gansel, M. Thiel, M. S. Rill, M. Decker, K. Bade, V. Saile, F. G. Von, S. Linden, and M. Wegener, Science **325**(5947), 1513–1515 (2009).
[13]Y. Zhao, M. A. Belkin, and A. Alù, Nat. Commun. **3**(3), 870 (2012).
[14]E. Plum, X. X. Liu, V. A. Fedotov, Y. Chen, D. P. Tsai, and N. I. Zheludev, Phys. Rev. Lett. **102**(11), 113902 (2009).
[15]M. Li, L. Guo, J. Dong, and H. Yang, J. Phys. D: Appl. Phys. **47**(18), 185102 (2014).
[16]C. Menzel, C. Helgert, C. Rockstuhl, E.-B. Kley, A. Tünnermann, T. Pertsch, and F. Lederer, Phys. Rev. Lett. **104**(25), 253902 (2010).
[17]V. A. Fedotov, P. L. Mladyonov, S. L. Prosvirnin, A. V. Rogacheva, Y. Chen, and N. I. Zheludev, Phys. Rev. Lett. **97**(16), 167401–167404 (2006).
[18]C. Pfeiffer, C. Zhang, V. Ray, L. J. Guo, and A. Grbic, Phys. Rev. Lett. **113**(2), 023902 (2014).
[19]E. Hendry, T. Carpy, J. Johnston, M. Popland, R. V. Mikhaylovskiy, A. J. Lapthorn, S. M. Kelly, L. D. Barron, N. Gadegaard, and M. Kadodwala, Nat. Nanotechnol. **5**(11), 783–787 (2010).
[20]Y. Tang and A. E. Cohen, Science **332**(6027), 333–336 (2011).
[21]Y. Tang and A. E. Cohen, Phys. Rev. Lett. **104**(16), 163901 (2010).
[22]N. Yu and F. Capasso, Nat. Mater. **13**(2), 139–150 (2014).
[23]P. Genevet, N. Yu, F. Aieta, J. Lin, M. A. Kats, R. Blanchard, M. O. Scully, Z. Gaburro, and F. Capasso, Appl. Phys. Lett. **100**(1), 013101 (2012).
[24]N. Yu, F. Aieta, P. Genevet, M. A. Kats, Z. Gaburro, and F. Capasso, Nano Lett. **12**(12), 6328–6333 (2012).
[25]A. Pors, M. G. Nielsen, R. L. Eriksen, and S. I. Bozhevolnyi, Nano Lett. **13**(2), 829–834 (2013).
[26]X. Chen, L. Huang, H. Mühlenbernd, G. Li, B. Bai, Q. Tan, G. Jin, C. W. Qiu, S. Zhang, and T. Zentgraf, Nat. Commun. **3**(6), 1198 (2012).
[27]N. Yu, P. Genevet, M. A. Kats, F. Aieta, J. P. Tetienne, F. Capasso, and Z. Gaburro, Science **334**(6054), 333–337 (2011).
[28]X. Ni and V. M. Shalaev, Science **335**(6067), 427 (2012).
[29]F. Aieta, M. A. Kats, P. Genevet, and F. Capasso, Science **347**(6228), 1342–1345 (2015).
[30]Y. Guo, Y. Wang, M. Pu, Z. Zhao, X. Wu, X. Ma, C. Wang, L. Yan, and X. Luo, Sci. Rep. **5**, 8434 (2015).
[31]L. Huang, X. Chen, H. Mühlenbernd, G. Li, B. Bai, Q. Tan, G. Jin, T. Zentgraf, and S. Zhang, Nano Lett. **12**(11), 5750–5755 (2012).
[32]L. Liu, X. Zhang, M. Kenney, X. Su, N. Xu, C. Ouyang, Y. Shi, J. Han, W. Zhang, and S. Zhang, Adv. Mater. **26**(29), 5031–5036 (2014).
[33]G. Zheng, H. Mühlenbernd, M. Kenney, G. Li, T. Zentgraf, and S. Zhang, Nat. Nanotechnol. **10**(4), 308–312 (2015).
[34]Z. Wang, K. Yao, M. Chen, H. Chen, and Y. Liu, Phys. Rev. Lett. **117**(15), 157401 (2016).
[35]J. Lin, J. P. Mueller, Q. Wang, G. Yuan, N. Antoniou, X. C. Yuan, and F. Capasso, Science **340**(6130), 331–334 (2013).
[36]S. Sun, Q. He, S. Xiao, Q. Xu, X. Li, and L. Zhou, Nat. Mater. **11**(5), 426–431 (2012).
[37]Z. Wang, H. Jia, K. Yao, W. Cai, H. Chen, and Y. Liu, ACS Photonics **3**(11), 2096–2101 (2016).
[38]E. Plum and N. I. Zheludev, Appl. Phys. Lett. **106**(22), 221901 (2015).
[39]W. Li, Z. J. Coppens, L. V. Besteiro, W. Wang, A. O. Govorov, and J. Valentine, Nat. Commun. **6**, 8379 (2015).
[40]V. A. Fedotov, A. V. Rogacheva, N. I. Zheludev, P. L. Mladyonov, and S. L. Prosvirnin, Appl. Phys. Lett. **88**(9), 091119 (2006).